IQ Imbalance Correction in Wideband Software Defined Radio Transceivers

Borisav JOVANOVIC [1,2], *Srdan MILENKOVIC* [1,2]

[1] Dept. of Electronics, Faculty of Electronic Engineering, University of Niš, Aleksandra Medvedeva 14, Niš, Serbia
[2] Lime Microsystems, Surrey Tech Centre, Occam Road, Guildford GU2 7YG, Surrey, UK

borisav.jovanovic@elfak.ni.ac.rs

Submitted July 5, 2023 / Accepted September 21, 2023 / Online first October 17, 2023

Abstract. *A method for compensation of frequency-selective (FS) in-phase/quadrature (IQ) imbalance of a wideband transceiver is proposed in the paper. It is dedicated for implementation in software defined radio (SDR) cellular base stations. Both transmitter (TX) and receiver (RX) IQ impairments are corrected by complex valued finite impulse response (FIR) filters which are designed based on previously found imbalance correction models. The compensation performance is assessed after the method was implemented in the SDR platform capable of transmitting signals at different central frequencies. At frequencies higher than 3 GHz measured IQ gain and phase error functions exhibit asymmetrical characteristic. In order to reduce the level of asymmetry, adopted IQ gain correction model incorporates odd polynomial elements while the phase correction model includes even polynomial parts. Regardless of utilized central frequency IQ impairments are efficiently compensated. The advantage of the proposed method is low complexity. The method doesn't require specialized hardware for calibration, instead, it uses the RF loopback. At central frequency of 3.5 GHz, transmitter image rejection ratio (IRR) is increased from 20 dBc to 45–50 dBc by applying the proposed method. After receiver imbalance is compensated, the improvement in IRR of more than 25 dBc is achieved.*

Keywords

Frequency selective IQ imbalance, transmitter, receiver, software defined radio, IQ calibration

1. Introduction

In ideal case, quadrature mixing in radio frequency (RF) transceivers completely suppresses image frequency components [1], [2]. In-phase/quadrature (IQ) imbalances, caused by degraded symmetry between I and Q signal paths, reflect in the path's unequal frequency responses. Uneven amplitudes of quadrature mixer local oscillator (LO) signals, and their phase shift, which is not equal to 90 degrees, additionally contribute the imbalance. It is proven that even with careful RF transceiver design only 30 to 40 dBc of image suppression can be achieved [1], [3].

The utilization of a static IQ imbalance (IQI) mitigation method is sufficient for calibration of narrowband transceivers. When wideband waveforms are transmitted the IQI becomes frequency selective (FS) and more computationally complex methods are required for compensation. The IQI mitigation is an important part of fifth generation (5G) transceiver design. Imbalance deteriorates the error vector magnitude (EVM) for which the 5G standards have strict requirements [4].

This paper presents a novel IQI reduction method which is dedicated to wideband transceivers. Both receiver and transmitter IQI are corrected. The method is implemented in a software defined radio (SDR) board. The utilized SDR supports different multi communication standards, frequency carriers and channel bandwidths. The particular requirement of the SDR is to transmit modulation waveforms having 100 MHz bandwidth while operating at 3.5 GHz central frequency. Initial SDR board measurements revealed significant IQ imbalance and emphasized the necessity for efficient IQI compensation method. Novel IQI reduction method is developed, realized using complex valued digital filters which are added to the digital baseband processing blocks. Steps for IQI mitigation are thoroughly described, starting from mathematical models to a complete realization in the SDR.

This paper is organized as follows. Related work is given in the following section. In Sec. 3, the method is described. In Sec. 4, implementation is presented followed by measured results. Section 5 is dedicated for discussion. The conclusion is drawn in the last section.

2. Related Work

The IQI includes the contributions from the analogue-to-digital converter (ADCs), digital-to-analogue converters (DACs), the analogue low-pass filters (LPFs), as well as the signal paths [3]. Refs. [5–7] investigate the mismatches between LPFs of I and Q signal paths as a source of the FS imbalance. In order to equalize the LPF frequency re-

DOI: 10.13164/re.2023.0479

sponses, additional feedback path, consisting of ADC, is embedded to the transceiver design. The feedback path returns the transmitter output signal to the baseband processing unit for IQI identification [6], [7]. The imbalance is mitigated using digital filters which are added to the digital baseband processing blocks [5], [7]. In [7] the test sequence is transmitted and fed back, while the operations are performed at transceiver start-up. The least squares (LS) optimization method is employed to minimize the difference between the desired filter response and the measured one. The reference [6] extends the operation of IQI correction circuits of [7] in order to be adaptive. Also, the imbalance is neutralized during transceiver operation. In [8], [9] the LS time domain approach is used for transmitter impairments identification. The impairments are reduced in the baseband using complex-valued finite impulse response (FIR) filters.

The IQI is detrimental to the digital predistortion (DPD) performance [10]. Many publications combine the IQI reduction with DPD power amplifier (PA) linearization. Such methods extend the parallel Hammerstein structure [11], Volterra series model [12] and asymmetrical complexity-reduced Volterra series model [13] to reduce both the transmitter IQ imbalance and PA nonlinearities. Impairments are cancelled using the complex-valued filters and DPD monitoring paths [10–13]. Although efficient, methods suffer from an increase in computational complexity of complex-valued filters compared to independent IQI compensation [14].

The IQI calibration algorithms can be divided into training sequence methods and blind methods according to whether the test signals are generated during calibration. Blind calibration does not require special test signals. Instead, it exploits the inherent characteristics of the received signal to calculate the imbalance parameters. Blind calibration can be based on blind source separation (BSS) techniques [15] and on signal statistical characteristics [15], [16].

The authors of [17] proposed a new adaptive algorithm for imbalance neutralization of receivers, which is based on backward blind source separation (BBSS) structure and the fast Newton transversal filter (FNTF) technique. In [18] a blind calibration method is applied for receiver's imbalance reduction. The frequency-domain statistical characteristics of the received signal are used for the construction of the classification rule that estimates the imbalance parameters. A real-valued digital filter is added to I component path to cancel the IQI. For method validation the gain and phase imbalances are generated using mismatched data. Reference [19] corrects the IQ impairments of an arbitrary waveform generator. The solution is based on a complex-valued filter whose structure is adopted from [9]. Method performance is assessed by laboratory measurements where the RF signal is acquired by high-performance oscilloscope and uploaded to a PC for IQI estimation. Reference [20] presents the IQ calibration method for ultra-wideband SDR zero-IF receivers, based on utilization of complex valued filters. The receiver has been equipped with an additional RF signal generator producing single tone test signals. Reference [21] utilizes the cross-power spectrum between I and Q signals to cancel the linear phase IQI consisting of the time delay deviation and the LO phase offset. The IQ amplitude mismatch and phase mismatch are reduced separately. The previous work [22] is based on memory polynomial DPD which jointly compensates transmitter IQI and PA nonlinearities. Transmitted signal bandwidth is limited by DPD operation which requires that the DAC/ADC sampling frequency is at least five times greater than the signal bandwidth. The maximum signal bandwidth of 20 MHz is achieved [22].

The methods found in literature are mostly validated in laboratory using test equipment that relies on high-performance instruments and state-of-the-art transceiver development boards. Also, the captured signals are imported to MATLAB where algorithms are carried out.

The main contributions of the proposed method are:

- IQ imbalance calibration method, dedicated for wideband transceivers, utilizes the test tones and has advantage that both transmitter and receiver are compensated in the same process.
- Beside the IQ imbalance compensation, amplitude responses are flattened. Impairments are compensated for 100 MHz signal bandwidth.
- The method was successfully implemented in a SDR board capable of transmitting waveforms at different LO frequencies. The measured results showed that at frequencies higher than 3 GHz the IQ gain and phase error functions exhibit asymmetrical characteristic. The imbalance is mitigated using complex-valued filters [9], [19]. Regardless of selected LO frequency, and the level of asymmetry in IQ imbalance functions, the IQ impairments are efficiently compensated.
- The method doesn't require specialized hardware for calibration; it uses the RF loopback instead.

3. Method for IQ Imbalance Correction

3.1 The Polynomial Models of Gain, IQ Gain and Phase Imbalance

Exposed to the source of IQI, the complex-valued signal $x(n)$, composed of quadrature components $x_I(n)$ and $x_Q(n)$, is transformed into $y(n)$, consisting of components denoted with $y_I(n)$ and $y_Q(n)$:

$$\begin{aligned} y_I(n) &= x_I(n)\cdot G_I(\omega)\cos(\omega n+\varphi_I(\omega)), \\ y_Q(n) &= x_Q(n)\cdot G_Q(\omega)\sin(\omega n+\varphi_Q(\omega)). \end{aligned} \tag{1}$$

We denote the gain of the I and Q channels as $G_I(\omega)$ and $G_Q(\omega)$, respectively. $\varphi_I(\omega)$ and $\varphi_Q(\omega)$ are corresponding channel phases. ω is the normalized angular frequency given by:

$$\omega = 2\pi \frac{f_C}{f_S} \tag{2}$$

where f_C is the signal carrier frequency and f_S is the sampling frequency. Transceiver's amplitude response should be a constant value, at least in the pass-band of interest. The amplitude function $G_I(\omega)$ is taken for a gain function, denoted with $g(\omega)$. With the increase of signal bandwidth, and also, with the increase of the transceiver's LO central frequency, the $g(\omega)$ becomes frequency dependent and improvement of $g(\omega)$ flatness is required.

The IQI is described via imbalance gain and phase functions. The IQI gain function $\gamma(\omega)$ is defined by [1]:

$$\gamma(\omega) = \frac{G_I(\omega)}{G_Q(\omega)}. \tag{3}$$

The phase imbalance $\varphi(\omega)$ is defined as the difference between I and Q component phases [1]

$$\varphi(\omega) = \varphi_I(\omega) - \varphi_Q(\omega). \tag{4}$$

The imbalance has a significant impact on the transceiver performance, which leads to the incomplete image signal rejection. For quantification of IQI effects the image rejection ratio (IRR) can be used. The IRR is defined as the ratio between the intermediate-frequency (IF) signal amplitude, produced by the desired input frequency and signal amplitude generated by the image frequency. For a given $\gamma(\omega)$ and $\varphi(\omega)$, the IRR is equal to [1]:

$$IRR(\omega) = 10\log\frac{1+\gamma(\omega)^2 + 2\gamma(\omega)\cos\varphi(\omega)}{1+\gamma(\omega)^2 - 2\gamma(\omega)\cos\varphi(\omega)}. \tag{5}$$

With increase of signal bandwidth, $\gamma(\omega)$ and $\varphi(\omega)$ become FS and IQI must be neutralized in the baseband using digital filters. This is the approach we follow. However, the filter design can be simplified when polynomial models for $g(\omega)$, $\gamma(\omega)$ and $\varphi(\omega)$ are designed first. Namely, many points of the desired filter amplitude and group delay responses will not be measured. Instead, they are calculated based on previously found models $g(\omega)$, $\gamma(\omega)$ and $\varphi(\omega)$. The advantage of this approach resides in reduced number of measurement points which speeds up the filter design and whole calibration process.

The circuits with real valued components have positive symmetrical amplitude response around the DC, and also, negative symmetrical phase response [2]. In this case, $\gamma(\omega)$ is constrained to be an even polynomial of ω, while $\varphi(\omega)$ (after removal of the DC phase offset) an odd polynomial. The correction circuits can be constructed using two real valued digital filters which are positioned in I and Q signal paths. However, in the RF, the symmetry may be degraded. It was seen by measurements that utilized SDR transceiver reveals asymmetric $\gamma(\omega)$ and $\varphi(\omega)$. To overcome this, the operation of complex-valued filters is required [9].

The amplitude response $g(\omega)$ of the circuit with real valued components is modeled by even function:

$$g(\omega) = a_0 + a_2\omega^2 + a_4\omega^4. \tag{6}$$

Symmetric form for IQI gain is given by:

$$\gamma_{\text{even}}(\omega) = b_0 + b_2\omega^2 + b_4\omega^4. \tag{7}$$

The asymmetric gain IQI function $\gamma(\omega)$ is:

$$\gamma(\omega) = b_0 + b_1\omega + b_2\omega^2 + b_3\omega^3 + b_4\omega^4. \tag{8}$$

The symmetric phase imbalance function is modeled with odd polynomial:

$$\varphi_{\text{odd}}(\omega) = c_0 + c_1\omega + c_3\omega^3. \tag{9}$$

The phase IQI model is modified to have asymmetric form:

$$\varphi(\omega) = c_0 + c_1\omega + c_2\omega^2 + c_3\omega^3 + c_4\omega^4. \tag{10}$$

The coefficients with index zero in the polynomials given by (6–10) represent the static gain and phase values. While static gain IQI is taken into account by desired amplitude responses, static phase imbalance is omitted from desired phase responses and is cancelled by a static phase correction block.

In order to find the $g(\omega)$, $\gamma(\omega)$ and $\varphi(\omega)$ coefficients sets of measurements are performed at angular frequencies ω_i, $i = 0,1,...,N$, uniformly distributed over baseband bandwidth range. The frequency values are selected on both sides around the DC. For each ω_i, the values for g_i, γ_i and φ_i are determined. The method for g_i, γ_i and φ_i calculation will be explained later in detail in the implementation section. Based on measured values g_i, γ_i and φ_i, the polynomial coefficients are calculated after mean square error (MSE) is minimized between measured data and polynomial models. The $g(\omega)$ coefficients are found after the following system of equations is solved:

$$\begin{bmatrix} s_0 & s_2 & s_4 \\ s_2 & s_4 & s_6 \\ s_4 & s_6 & s_8 \end{bmatrix} \begin{bmatrix} a_0 \\ a_2 \\ a_4 \end{bmatrix} = \begin{bmatrix} \sum_{i=0}^{N} g_i & \sum_{i=0}^{N} g_i\omega_i^2 & \sum_{i=0}^{N} g_i\omega_i^4 \end{bmatrix}^{\mathrm{T}}. \tag{11}$$

The elements s_j are defined as:

$$s_j = \sum_{i=0}^{N} \omega_i^j. \tag{12}$$

Similarly, the $\gamma(\omega)$ and $\varphi(\omega)$ coefficients are found after systems of equations given by (13), (14) are solved:

$$\left[s_{k+l-2}\right]_{k,l=1,...,5} \left[b_{j-1}\right]_{j=1,...,5}^{\mathrm{T}} = \left[\sum_{i=0}^{N} \gamma_i\omega_i^{j-1}\right]_{j=1,...,5}^{\mathrm{T}}, \tag{13}$$

$$\left[s_{k+l-2}\right]_{k,l=1,...,5} \left[c_{j-1}\right]_{j=1,...,5}^{\mathrm{T}} = \left[\sum_{i=0}^{N} \varphi_i\omega_i^{j-1}\right]_{j=1,...,5}^{\mathrm{T}}. \tag{14}$$

3.2 The FIR Filter Specification

The block diagram of the circuit dedicated for IQ correction is depicted in Fig. 1. The correction scheme is based on a complex FIR filter adopted from [9]. The circuit is composed of four real valued FIR filters. The FIR_II and FIR_QQ are positioned in I and Q signal paths. The other two, the FIR_IQ and FIR_QI, are located in the cross paths. The digital filters have length M. Besides, separate correctors are dedicated for receiver and transmitter IQI mitigation.

For the construction of FIR_IQ and FIR_QI the digital differentiator FIR filters are used whose length M is an odd number. The frequency response of a digital differentiator is given by [23]:

$$H_{\text{diff}}(\omega) = K \cdot \mathrm{j}\omega \tag{15}$$

where the parameter K represents its gain. The impulse response is given by [23]:

$$h_{\text{diff}}(n) = \begin{cases} K \dfrac{\cos(\pi(n-\alpha))}{n-\alpha}, n \neq \alpha \\ 0, n = \alpha \end{cases} \tag{16}$$

where $\alpha = (M - 1)/2$. In an effort to improve amplitude response linearity the filter coefficients from (16) are modified by the Hamming window function [23].

In IQI analysis we assume that the signals at the inputs X_{I} and X_{Q} (given in Fig. 1) are equal to $\cos(\omega_0 n)$ and $\sin(\omega_0 n)$ and the K is a positive value. Also, we assume that the filters FIR_II and FIR_QQ are bypassed (their outputs are delayed for the delay of FIR filters and not changed in gain and phase).

Using Euler's complex expansion of cosine and sine functions, the signals X_{I} and X_{Q} can be represented as a sum of two components positioned at ω_0 and $-\omega_0$:

$$\begin{aligned} X_{\text{I}} &= \cos(\omega_0 n) = \frac{1}{2}\exp(\mathrm{j}\omega_0 n) + \frac{1}{2}\exp(-\mathrm{j}\omega_0 n), \\ X_{\text{Q}} &= \sin(\omega_0 n) = \frac{\mathrm{j}}{2}\exp(-\mathrm{j}\omega_0 n) - \frac{\mathrm{j}}{2}\exp(\mathrm{j}\omega_0 n). \end{aligned} \tag{17}$$

The FIR_IQ modifies X_{I} into X_{IQ}, while the FIR_QI produces at its output X_{QI}. The graphical representation of X_{I}, X_{Q}, X_{IQ} and X_{QI} decomposition is shown in Fig. 2. The X_{IQ} components amplitudes are $0.5K\omega_0$ and $-0.5K\omega_0$, at ω_0 and $-\omega_0$. In the case of X_{QI} they are both equal to $0.5K\omega_0$. The FIR_QI increases the gain in I path by $0.5K\omega_0$ while the Q path gain is reduced by the same amount. The gain imbalance is $(1 + K\omega_0) / (1 - K\omega_0)$.

The gain imbalance, induced by FIR_IQ and FIR_QI, is equalized with the odd gain imbalance function $\gamma_{\text{odd}}(\omega)$:

$$1 + \gamma_{\text{odd}}(\omega) = 1 + \mathrm{b}_1\omega + \mathrm{b}_3\omega^3 = \frac{1+\omega K(\omega)}{1-\omega K(\omega)}. \tag{18}$$

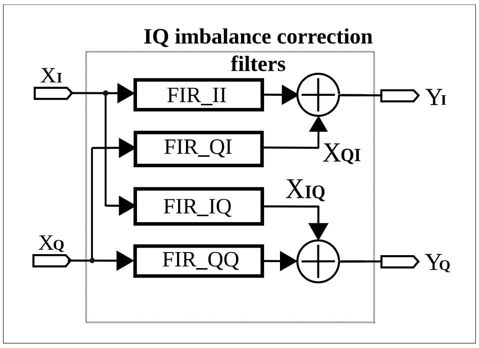

Fig. 1. The IQ compensator architecture.

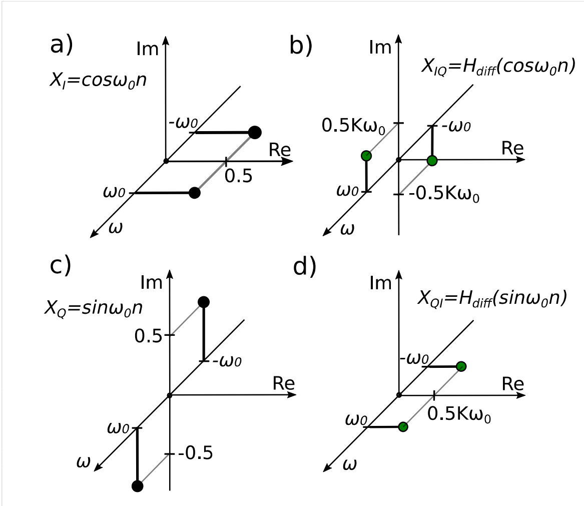

Fig. 2. The frequency components of a) the FIR_IQ input, b) the FIR_IQ output, c) FIR_QI input and d) FIR_QI output.

$K(\omega)$ is calculated by:

$$K(\omega) = \frac{b_1 + b_3\omega^2}{2 + b_1\omega + b_3\omega^3}. \tag{19}$$

The asymmetrical $\varphi_{\text{even}}(\omega)$ is corrected by a phase imbalance produced by a time delay between FIR_IQ and FIR_QI impulse responses. Namely, when impulse response of FIR_QI is delayed relative to the response of FIR_IQ, the signal at I path output is given by:

$$\begin{aligned} Y_{\text{I}} &= \cos(\omega n) + \omega K(\omega)\cos(\omega n - 2\pi\omega \cdot delay) = \\ &\cos(\omega n) \cdot (1 + \omega K(\omega)\cos(2\pi\omega \cdot delay)) + \\ &\sin(\omega n) \cdot \omega K(\omega)\sin(2\pi\omega \cdot delay). \end{aligned} \tag{20}$$

The introduced phase shift neutralizes the $\varphi_{\text{even}}(\omega)$:

$$\begin{aligned} \varphi_{\text{even}}(\omega) &= c_2\omega^2 + c_4\omega^4 = \\ &\arctan\left(\frac{\omega K(\omega) \cdot \sin(2\pi\omega \cdot delay)}{1 + \omega K(\omega) \cdot \cos(2\pi\omega \cdot delay)}\right). \end{aligned} \tag{21}$$

The delay value, expressed in $1/f_{\text{S}}$ units, is calculated from (21) and it is used for the construction of a fractional delay (FD) FIR filter [21] whose frequency response is denoted with $H_{\mathrm{sinc}}(\omega, delay)$. The FD filter and digital differentiator share the same filter length.

The impulse response $h_{\mathrm{sinc}}(n, delay)$ is given by [23]:

$$h_{\mathrm{sinc}}\left(n, delay\right) = \begin{cases} \dfrac{\sin\left(\pi\left(n-\alpha-delay\right)\right)}{n-\alpha-delay}, & n-\alpha-delay \neq 0, \\ 1, & n-\alpha-delay = 0. \end{cases} \tag{22}$$

The amplitude response $K(\omega)$ from (21) is approximated by an FIR filter named FIR_K. The desired amplitude and phase responses of FIR_K are specified by:

$$\begin{aligned} A_{\mathrm{FIR\_K}}(\omega) &= K(\omega), \\ \varphi_{\mathrm{FIR\_K}}(\omega) &= 0, \\ \tau_{\mathrm{FIR\_K}}(\omega) &= 0. \end{aligned} \tag{23}$$

The FIR_IQ and FIR_QI are produced by convolution of three filters: the digital differentiator, FIR_K and FD:

$$\begin{aligned} H_{\mathrm{FIR\_IQ}}(\omega, delay) &= \mathrm{j}\omega * K(\omega) * H_{\mathrm{sinc}}(\omega, 0), \\ H_{\mathrm{FIR\_QI}}(\omega) &= \mathrm{j}\omega * K(\omega) * H_{\mathrm{sinc}}(\omega, delay). \end{aligned} \tag{24}$$

The odd function $\varphi_{\mathrm{odd}}(\omega)$ is compensated by FIR_II whose amplitude response contains the inverse of $g(\omega)$. The FIR_II filter is described by:

$$g_{\mathrm{FIR\_II}}\left(\omega\right) = \frac{1}{g\left(\omega\right)}, \quad \varphi_{\mathrm{FIR\_II}}\left(\omega\right) = \varphi_{\mathrm{odd}}\left(\omega\right). \tag{25}$$

The $\gamma_{\mathrm{even}}(\omega)$ is corrected by FIR_QQ. The amplitude response of FIR_QQ contains the inverse of $g(\omega)$. The desired amplitude and phase responses are given by:

$$\begin{aligned} g_{\mathrm{FIR\_QQ}}\left(\omega\right) &= \frac{\gamma_{\mathrm{even}}\left(\omega\right)}{g\left(\omega\right)}, \\ \varphi_{\mathrm{FIR\_QQ}}\left(\omega\right) &= 0. \end{aligned} \tag{26}$$

Splitting the operations for correction of $\gamma_{\mathrm{even}}(\omega)$ and $\varphi_{\mathrm{odd}}(\omega)$ between FIR_II and FIR_QQ relaxes filter specification, and consequently, reduces the number of filtering taps. By substituting $\gamma_{\mathrm{even}}(\omega)$ and $\varphi_{\mathrm{odd}}(\omega)$, the FIR_II amplitude and group delay become:

$$\begin{aligned} A_{\mathrm{FIR\_II}}\left(\omega\right) &= \frac{1}{a_0 + a_2\omega^2 + a_4\omega^4}, \\ \tau_{\mathrm{FIR\_II}}\left(\omega\right) &= -\frac{1}{Ts}\frac{\mathrm{d}\varphi_{dI}\left(\omega\right)}{\mathrm{d}\omega} = \frac{c_1 + 3c_3\omega^2}{2\pi}. \end{aligned} \tag{27}$$

Similarly, the FIR_QQ amplitude and group delay are specified by:

$$\begin{aligned} A_{\mathrm{FIR\_QQ}}\left(\omega\right) &= \frac{b_0 + b_2\omega^2 + b_4\omega^4}{a_0 + a_2\omega^2 + a_4\omega^4}, \\ \tau_{\mathrm{FIR\_QQ}}\left(\omega\right) &= 0. \end{aligned} \tag{28}$$

3.3 Amplitude and Phase Response, the Group Delay of FIR Filter

The transfer function of M tap FIR filters is given by:

$$H\left(z\right) = \sum_{k=0}^{M-1} h_k z^{-k}. \tag{29}$$

The frequency response of the filter has the form:

$$H\left(\omega\right) = R\left(\omega\right) - \mathrm{j}I\left(\omega\right), \tag{30}$$

while the real and imaginary parts are calculated as:

$$\begin{aligned} R\left(\omega\right) &= \sum_{k=0}^{M-1} h_k \cos\left(k\omega\right), \\ I\left(\omega\right) &= \sum_{k=0}^{M-1} h_k \sin\left(k\omega\right). \end{aligned} \tag{31}$$

The amplitude and phase of the complex function are:

$$\begin{aligned} A\left(\omega\right) &= \sqrt{R\left(\omega\right)^2 + I\left(\omega\right)^2}, \\ \varphi\left(\omega\right) &= \arg H\left(\omega\right) = -\arctan\frac{I\left(\omega\right)}{R\left(\omega\right)}. \end{aligned} \tag{32}$$

Finally, the normalized group delay is given as:

$$\tau\left(\omega\right) = -\frac{\partial\varphi\left(\omega\right)}{\partial\omega} = -\frac{R\left(\omega\right)R_k\left(\omega\right) + I\left(\omega\right)I_k\left(\omega\right)}{R\left(\omega\right)^2 + I\left(\omega\right)^2}, \tag{33}$$

$$\begin{aligned} R_k\left(\omega\right) &= \sum_{k=0}^{M-1} h_k k \cos\left(k\omega\right), \\ I_k\left(\omega\right) &= \sum_{k=0}^{M-1} h_k k \sin\left(k\omega\right). \end{aligned} \tag{34}$$

3.4 Iterative Procedure for Coefficients Calculation

Identical numerical optimization procedures are used for construction of FIR_K, FIR_II and FIR_QQ. The coefficients are determined under two constraints. In the first, the amplitude response $A(\omega)$ from (32) should approximate $A_{\mathrm{FIR\_K}}(\omega)$, $A_{\mathrm{FIR\_II}}(\omega)$ and $A_{\mathrm{FIR\_QQ}}(\omega)$ for filters FIR_K, FIR_II and FIR_QQ, respectively. The second constraint considers the group delay $\tau(\omega)$ from (33) which is made to be as close as possible to $\tau_{\mathrm{FIR\_K}}(\omega)$, $\tau_{\mathrm{FIR\_II}}(\omega)$ and $\tau_{\mathrm{FIR\_QQ}}(\omega)$.

In the signal pass band, P frequency points are selected. $P_s - 1$ out of band frequency points are chosen as well and the desired amplitude response is constrained for $A(\omega)$. Out-of-band amplitude constraint prevents the resulting amplitude response to have large out-of-band gain which may produce data overflow when the filter is implemented. An arbitrary weighting function $A_w(\omega)$ is used to control the approximation accuracy in certain frequency bands. For example, out-of-band $A_w(\omega)$ can be set to a very small value which in turn improves in-band amplitude response approximation.

Group delay constraint is defined in a similar way. Here, $\tau(\omega)$ and $\tau_w(\omega)$ represent target group delay and group delay weighting function, respectively. The group delay constraint is defined only for the signal pass band.

Based on the above definitions, the cost function is constructed to minimize the difference between the desired response and that measured from I and Q channels respectively.

$$\begin{aligned} E &= \frac{\lambda}{2}\sum_{l=1}^{P-1}\tau_{\mathrm{w}}(\omega_l)\left(\tau(\omega_l)-\tau_{\mathrm{d}}(\omega_l)-\beta\right)^2 \\ &+\frac{(1-\lambda)}{2}\sum_{l=1}^{P+P_s-1}A_{\mathrm{w}}(\omega_l)\left(A(\omega_l)-A_{\mathrm{d}}(\omega_l)\right)^2. \end{aligned} \tag{35}$$

There are two more coefficients introduced in (35). Namely, λ is the penalty factor which defines relative importance of the amplitude and group delay constraints while β is an additional parameter which represents latency. It is fixed here to $(M-1)/2$ and is not changed during the optimization. The optimization problem defined by (35) is nonlinear and Davidon-Fletcher-Powell (DPF) method is used to solve it numerically [24].

The FIR coefficients are stored in the vector **h,** which elements are changed in an iterative DPF process.

$$\mathbf{h}(i)=\left[\,h_0(i)\quad h_1(i)\ldots\quad h_{M-1}(i)\right]. \tag{36}$$

The required DPF partial derivatives are calculated as follows:

$$\begin{aligned} \frac{\partial\varepsilon}{\partial h_k} &= \lambda\sum_{l=1}^{P-1}\tau_{\mathrm{w}}(\omega_l)\left(\tau(\omega_l)-\tau_{\mathrm{d}}(\omega_l)-\beta\right)\frac{\partial\tau(\omega_l)}{\partial h_k} \\ &+(1-\lambda)\sum_{l=1}^{P+P_s-1}A_{\mathrm{w}}(\omega_l)\left(A(\omega_l)-A_{\mathrm{d}}(\omega_l)\right)\frac{\partial A(\omega_l)}{\partial h_k}. \end{aligned} \tag{37}$$

The starting vector $\mathbf{h}(0)$ has all zero value elements. The DPF utilizes the identity matrix $\mathbf{I}$ which has $M\times M$ dimension. In every iteration $\mathbf{I}(i)$ elements are changed; in the starting point $\mathbf{I}(0)$ has all zero elements, except the elements on the main matrix diagonal which are equal to one. The gradient function is [24]:

$$\nabla f\left(\mathbf{h}(i)\right)=\left[\frac{\partial f}{\partial h_0}\quad\frac{\partial f}{\partial h_1}\quad\ldots\quad\frac{\partial f}{\partial h_{M-1}}\right]^{\mathrm{T}}_{\mathbf{h}=\mathbf{h}(i)}. \tag{38}$$

In iteration the vector **h** elements are changed for [24]:

$$\Delta\mathbf{h}(i)=\mathbf{h}(i+1)-\mathbf{h}(i)=-\eta\,\mathbf{I}\,\nabla f(\mathbf{h}(i)). \tag{39}$$

The parameter η is calculated from the constraint that the $f(\mathbf{h}(i+1))$ is minimized [24]. The change of gradient function value is [24]:

$$\Delta\mathbf{g}(i)=\nabla f(\mathbf{h}(i+1))-\nabla f(\mathbf{h}(i)). \tag{40}$$

The matrix $\mathbf{I}(i)$ is updated with [24]:

$$\mathbf{I}(i+1)=\mathbf{I}(i)+\frac{\Delta\mathbf{h}\Delta\mathbf{h}^{\mathrm{T}}}{\Delta\mathbf{h}^{\mathrm{T}}\nabla\mathbf{g}}-\frac{\mathbf{I}(i)\nabla\mathbf{g}\nabla\mathbf{g}^{\mathrm{T}}\mathbf{I}(i)}{\nabla\mathbf{g}^{\mathrm{T}}\mathbf{I}(i)\nabla\mathbf{g}}. \tag{41}$$

4. Implementation

The IQI correction method is validated through practical hardware implementation in the LimeSDR QPCIe SDR board [25]. The transceiver, whose IQ imbalance is calibrated, is LMS7002M IC [25]. The transceiver covers the central frequency range of several hundreds of MHz to 3.8 GHz [25]. The PC is equipped with the SDR board inserted in the peripheral component interconnect express (PCIe) slot. Beside the SDR, the measurement setup includes the spectrum analyzer and RF signal generator which are used in IRR measurements. In the setup the SDR TX output is connected via RF cable to the input of Keysight E4440 spectrum analyzer. The Keysight E8267D signal generator output is connected to RX input of the SDR board. The signal generator and spectrum analyzer are not used during the calibration process; they are utilized during IRR measurements.

The software consists of the LimeSuite [25], the software implementing digital modulator and the application dedicated to IQ calibration. The SDR is configured using LimeSuite. The configuration files are loaded into LMS7002M ICs [25], the on-board DAC and ADC sample rates are set to 245.76 MHz and 122.88 MHz, respectively. Upon loading the configuration files, the SDR transmitter and receiver are in uncalibrated state. The software implementing the digital modulator functions generates 100 MHz wideband waveforms at a rate of 122.88 MS/s and it is explained in [26] in detail.

The SDR board, whose block diagram is depicted in Fig. 3, includes two transceiver ICs, an Altera Cyclone V FPGA chip, 14-bit external ADC and DACs [25]. To increase the capacity of a radio link, two-by-two multiple-input and multiple-output (MIMO) transceiver is implemented on SDR board. The SDR board has many other options than shown in Fig. 3. For clarity, only minimum hardware blocks are presented in the figure, which are relevant for a method description.

The signals, generated by digital modem [26], are fed into the SDR board via PCIe at a rate of 122.88 MS/s and they are processed by transmit path (TX) signal processing blocks, as shown in Fig. 3.

An oversampling of factor one is used before the DACs, yielding a data rate of 245.76 MS/s. The data rate is constrained by DAC rate maximum of 250 MS/s. Transmitted signal bandwidth is 100 MHz and the interpolation block is required to eliminate unwanted DAC-related signal images. At the transmit side, the IQ samples pass through the signal interpolation block, the TX static IQI and

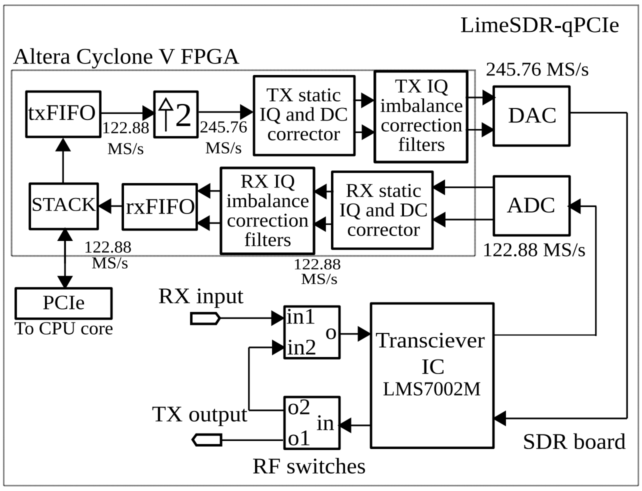

Fig. 3. The implementation platform.

DC offset correctors, followed by IQI compensators. The IQI correction filters operate at a sample rate of 245.76 MS/s. The 18-bit arithmetic precision does not impact the algorithm performance. The TX IQI compensator is composed of four 15-tap FIR filters whose structure is given in Fig. 1. For realization of one FIR filter the following FPGA resources are spent: 330 adaptive logic modules (ALM), 350 combinatorial adaptive look-up tables (ALUT), 700 dedicated registers and 9 DSP blocks. Frequency up conversion from baseband (BB) to RF and down conversion from RF to BB, are performed by transmitter and receiver chains.

At the receiving side, the signals are sampled by 14-bit ADCs at a rate of 122.88 MS/s. The data rate is constrained by on-board ADC maximum data rate of 160 MS/s. Signals are further processed by digital blocks implemented in FPGA. The receive (RX) chain blocks include the static IQ and DC correctors followed by RX IQI correction circuit which share identical structure as the circuit in TX path.

The IQI calibration procedures are executed at transceiver start-up. The board incorporates only a few additional circuits supporting the calibration process. These circuits consist of the RF switches that form the RF loopback path from transmitter output to receiver input. Therefore, the RF loopback introduces only minimal modifications in SDR hardware (i.e. no additional mixers, ADCs or other expensive monitoring equipment). In the calibration process the transmitter plays the role of a test signal generator while the receiver is used as a monitoring device. In each measurement point the IQI parameters are extracted by analyzing the received signal spectrum.

The complex filter coefficients are calculated by C/C++ software application that runs on a CPU core. Internally, the algorithm operations can be divided into calibration routines, the coefficient's calculation operations and FIR filter programming operations. After filter coefficients are calculated they are transferred to the SDR board via PCIe. The correction filters have provision to change their coefficients via the Serial Peripheral Interface (SPI). The coefficients are sent to the FPGA over the PCIe/SPI. In order to automate the IRR measurement operations, the functionality of software application is extended to control spectrum analyzer and RF signal generator via LAN connection. The application performs the RX and TX IRR measurements. After calibration is finished, the filter coefficients can be stored in a file. When the transceiver is powered up, the calibration process can be skipped. The coefficients are read from the recorded file and loaded into the complex filter registers.

4.1 The Calibration Routines

The receiver and transmitter imbalances are separately extracted. A calibration setup is used that was presented in [16]. This setup uses the single-frequency tones to calibrate the receiver and then proceeds to use the calibrated receiver as a measuring device. The transmitter supplies the test tones into the receiver over RF loopback. The test tones are generated either by transmitter LO or by numerically controlled oscillator (NCO) which is embedded in the TX static calibration block. The amplitudes of the signal and corresponding image tone are determined using spectral analysis. Besides, the static TX and RX IQ correctors are configured to minimize the amplitudes of unwanted images.

The block diagrams of RX and TX static IQ correctors are presented in Fig. 4. The transmitter's static IQ corrector parameters include gain correction codes (*txGain_I* and *txGain_Q*) and phase correction code (the *txAlpha*). Similarly, the RX static IQ corrector parameters include *rxGain_I*, *rxGain_Q* and *rxAlpha*.

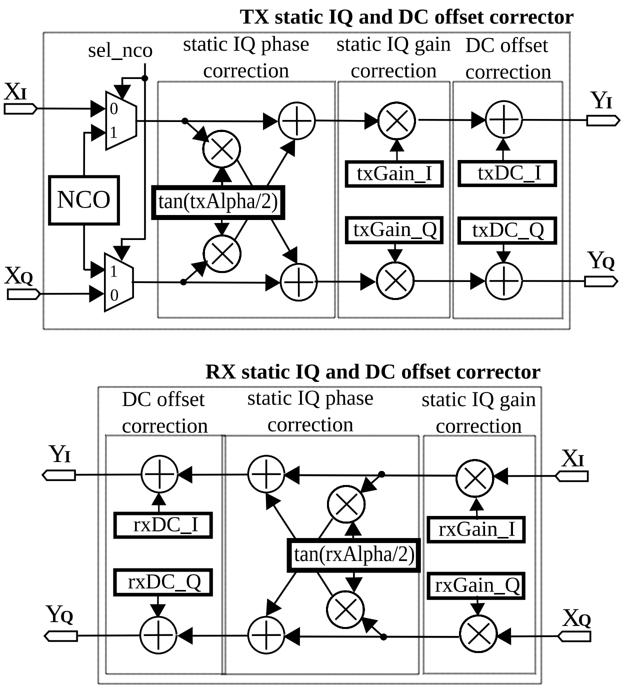

Fig. 4. Static IC IQI and DC offset correctors.

The following BB frequencies are selected for measurement points f_i [MHz] = {−50, −45, −40, −30, −20, −10, 10, 20, 30, 40, 45, 50}. The angular frequency values ω_i, $i = 0,1, \ldots,11$, are derived after f_i values are divided with sample rate values. For the transmitter, the sample rate is 245.76 MS/s while the receiver sample rate is equal to 122.88 MS/s. The calibration operations can be divided in phases designated as 1, 2 and 3. The calibration results are the values for gain - g_i and IQI parameters - γ_i and φ_i, which are obtained for each ω_i. The phases are explained as follows.

The calibration phase 1 is the preparation step for phase 2. In phase 1 the receiver is calibrated. The test tones are generated by transmitter LO. At the beginning of phase 1, the RX LO frequency is fixed to target TX LO frequency (the target TX f_{LO}) and is not changed further during phase 1. The RX DC offset is corrected.

The DC correction codes *rxDC*_1_*I* and *rxDC*_1_*Q* are calculated and programmed in the RX static IQ corrector (shown in Fig. 4). In each point, the test tone is generated by tuning the TX LO to the frequency equal to target $TX\_f_{\mathrm{LO}}+f_i$, where target TX_f_{LO} is a constant. After the RF loopback is established and data is read, a spectral analysis is performed over the received data. A desired signal component, observed at $f = f_i$, is accompanied by an undesired image, positioned at $f = -f_i$. The image signal amplitude is minimized by changing the parameters of the RX static IQ corrector. The phase 1 outputs, which correspond to f_i, are the RX gain ($rxGain\_1\_I_i$, $rxGain\_1\_Q_i$) and phase ($rxAlpha\_1_i$) correction codes. The described operations are repeated for all f_i.

In phase 2 the transmitter is calibrated. The test tones are generated by TX NCO located in the static TX IQ corrector block (Fig. 4). At phase 2 beginning, the TX and RX LO are set to target TX_f_{LO}. Then, the TX DC offset is calibrated. In each measurement point, the NCO frequency is set to f_i and RX IQ correction codes $rxGain\_1\_I_i$, $rxGain\_1\_Q_i$, $rxAlpha\_1_i$ are loaded into the RX IQ corrector. The RF loopback is formed and the amplitudes of signals positioned at f_i, and $-f_i$ are measured. The image signals are reduced by adjusting the TX static IQ corrector. The phase 2 results are correction codes for TX IQ gain ($txGain\_2\_I_i$, $txGain\_2\_Q_i$) and phase ($txAlpha\_2_i$). The IQI parameters tx_γ_i and tx_φ_i are calculated by (42), (43). The tx_g_i is found as the amplitude of the signal positioned at f_i, normalized to the amplitude maximum.

$$tx\_\gamma_i = \frac{txGain\_2\_Q_i}{txGain\_2\_I_i}, \tag{42}$$

$$tx\_\varphi_i = 2\cdot\arctan\left(\frac{txAlpha\_2_i}{2048}\right). \tag{43}$$

In phase 3, the RX IQI calibration procedure is repeated. The operations are similar to those executed in phase 1. The transmitter LO is again used as a tone generator. The RX LO is now tuned to the target RX f_{LO}. The RX DC offset is calibrated. In each point, the TX LO is tuned to the target $RX\_f_{\mathrm{LO}} + f_i$. The image signal is minimized by employing the RX static IQ corrector. For each f_i, the following corrector codes are acquired: $rxGain\_3\_I_i$, $rxGain\_3\_Q_i$ and $rxAlpha\_3_i$. The rx_γ_i and rx_φ_i are calculated by (44), (45). The rx_g_i is derived from the amplitude of the signal positioned at f_i.

$$rx\_\gamma_i = \frac{txGain\_3\_Q_i}{txGain\_3\_I_i}, \tag{44}$$

$$rx\_\varphi_i = 2\cdot\arctan\left(\frac{txAlpha\_3_i}{2048}\right). \tag{45}$$

The g_i, γ_i and φ_i values, gained for RX and TX at f_i, are used for calculation of the $g(\omega)$, $\gamma(\omega)$ and $\varphi(\omega)$ (using (11–14)). The mathematical background for conversion of the $g(\omega)$, $\gamma(\omega)$ and $\varphi(\omega)$ into the coefficients of FIR filters (the RX and TX FIR_II, FIR_QQ, FIR_K) is described in the previous section.

4.2 Transmitter Measurement

The method performance is estimated in cases when transmitter is tuned to different LO frequencies: TX_f_{LO} = {2.0 GHz, 2.3 GHz, 2.6 GHz, 2.9 GHz, 3.2 GHz and 3.5 GHz}. The calibration is performed for all f_{LO} from the set. The routines, described in Sec. 4.1, are executed for un-calibrated and calibrated transmitter in order to calculate the TX IQ gain and phase errors. The TX IQ gain and phase imbalance values are determined by (42) and (43).

Normalized amplitude response, as a function f_{LO} and f_{BB}, is given in Fig. 5. The curve labeled as “Meas.” is obtained by measured data before the proposed method is applied. The results, which are labeled as “Corr.” curves, represent corrected results, derived after the IQI is minimized. When amplitude response is considered, the results presented in the figure prove that the corrected amplitude response is flatter than the measured one. However, the corrected results are not ideally flat because only even polynomials are compensated.

Measured and corrected IQI phase values are shown in Fig. 6. In the most challenging case, when TX_f_{LO} = 3.5 GHz, the phase imbalance ranges from 8 degrees, obtained for $f_{\mathrm{BB}} = -50$ MHz, up to 16 degrees, gained for $f_{\mathrm{BB}} = 50$ MHz. As it can be seen from the figure, the corrected phase IQI is efficiently minimized, regardless of tuned TX_f_{LO}.

The gain IQI results, measured at different TX_f_{LO}, are given in Fig. 7. At lower TX_f_{LO} frequencies (up to 2.6 GHz) the measured IQI curves are symmetrical. When TX_f_{LO} is increased, the symmetry is degraded. After the method is applied, the gain IQI is efficiently reduced; the corrected values are very close to the ideal case.

The IRR results are acquired by measurements in which single tone test signals are generated by SDR transmitter NCO. The baseband signal is in the range f_{BB} = [−50 MHz, 50 MHz]. The transmitter output is observed

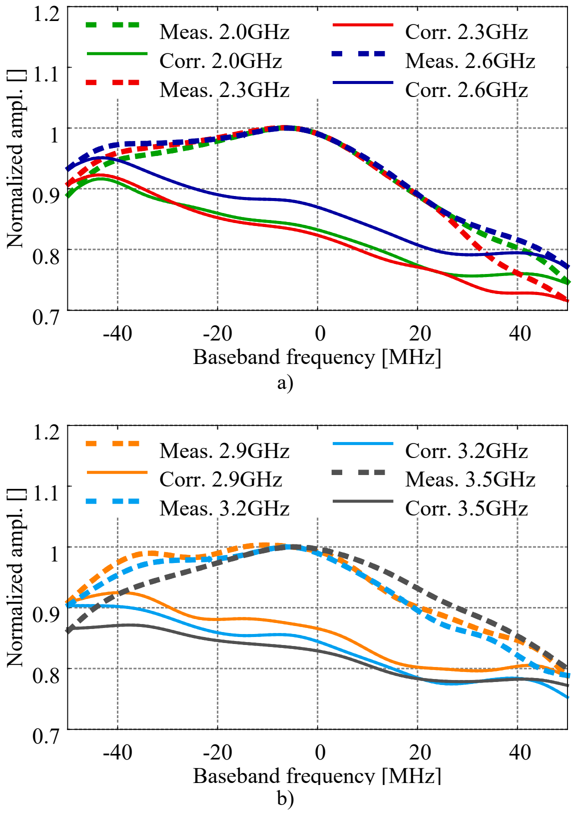

Fig. 5. Transmitter normalized measured and corrected amplitude response obtained at a) 2.0 GHz, 2.3 GHz, 2.6 GHz, b) 2.9 GHz, 3.2 GHz and 3.5 GHz.

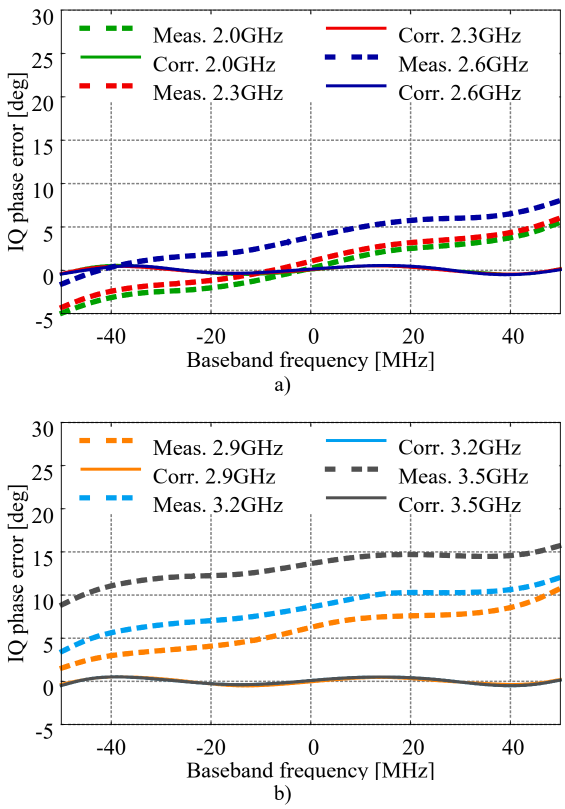

Fig. 6. Measured and corrected transmitter phase IQI functions acquired at: a) 2.0 GHz, 2.3 GHz, 2.6 GHz, b) 2.9 GHz, 3.2 GHz and 3.5 GHz.

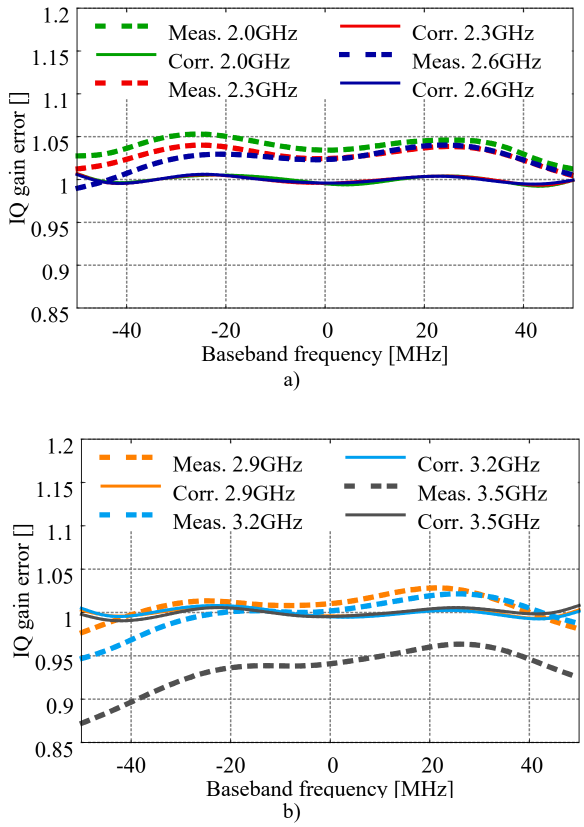

Fig. 7. Transmitter IQ gain imbalance at: a) 2.0 GHz, 2.3 GHz, 2.6 GHz, b) 2.9 GHz, 3.2 GHz, 3.5 GHz.

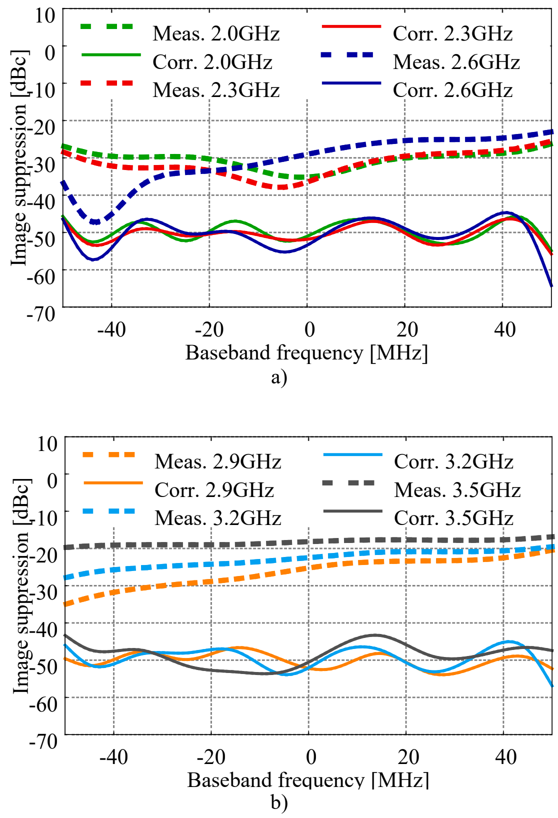

Fig. 8. TX IQI image level suppression at: a) 2.0 GHz, 2.3 GHz, 2.6 GHz, b) 2.9 GHz, 3.2 GHz and 3.5 GHz.

using a spectrum analyzer whose central frequency is set to TX_f_{LO}. The image suppression level (the inverse of IRR) as a function of f_{LO} and f_{BB} is shown in Fig. 8. The amplitude of the main test signal, positioned at $TX\_f_{LO}+f_{BB}$, and the image component, positioned at $TX\_f_{LO}-f_{BB}$, are measured. The IRR is determined by the difference between the amplitudes of the signal and its image. The IRR results clearly demonstrate an improvement in image rejection. When f_{LO} = 3.5 GHz and the method is not applied, the IRR is only 20 dBc. When IQI is reduced and the transceiver operates at the same f_{LO}, the IRR values ranges from 45 to 55 dBc. The enhancement in IRR is more than 25 dBc.

4.3 Receiver Measurement

The SDR receiver is calibrated and IQ imbalance is measured at LO frequencies RX_f_{LO}={2.0 GHz, 2.3 GHz, 2.6 GHz, 2.9 GHz, 3.2 GHz and 3.5 GHz}. The measurement routines, described in Sec. 4.1, are separately performed for un-calibrated and calibrated receiver in order to get measured and corrected RX IQ gain and phase imbalance values. The RX gain and phase imbalances are calculated using (44) and (45), respectively.

Normalized receiver amplitude response, as a function of f_{LO} and f_{BB}, is given in Fig. 9. The phase imbalance values are depicted in Fig. 10. As it can be seen from Fig. 10, at f_{LO} = 3.5 GHz the measured phase imbalance function shows asymmetry. The corrected phase imbalance values prove method efficiency in IQI reduction. The RX gain IQI is depicted in Fig. 11.

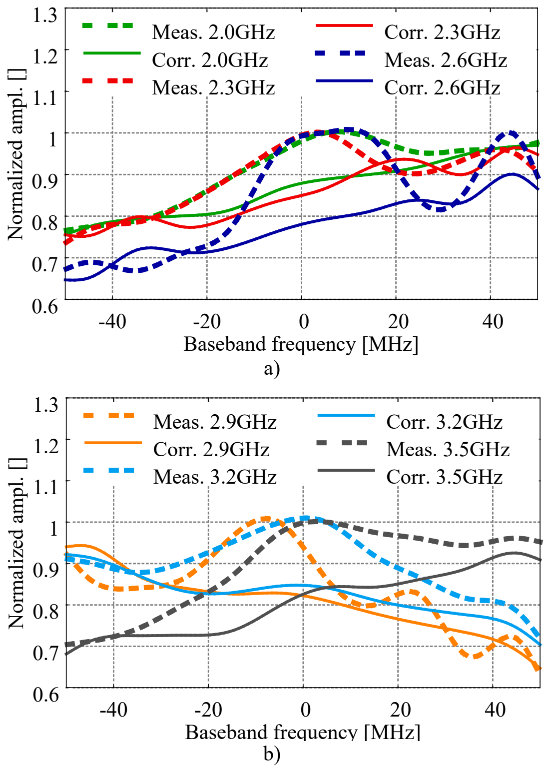

Fig. 9. RX normalized amplitude response at: a) 2.0 GHz, 2.3 GHz, 2.6 GHz; b) 2.9 GHz, 3.2 GHz, 3.5 GHz.

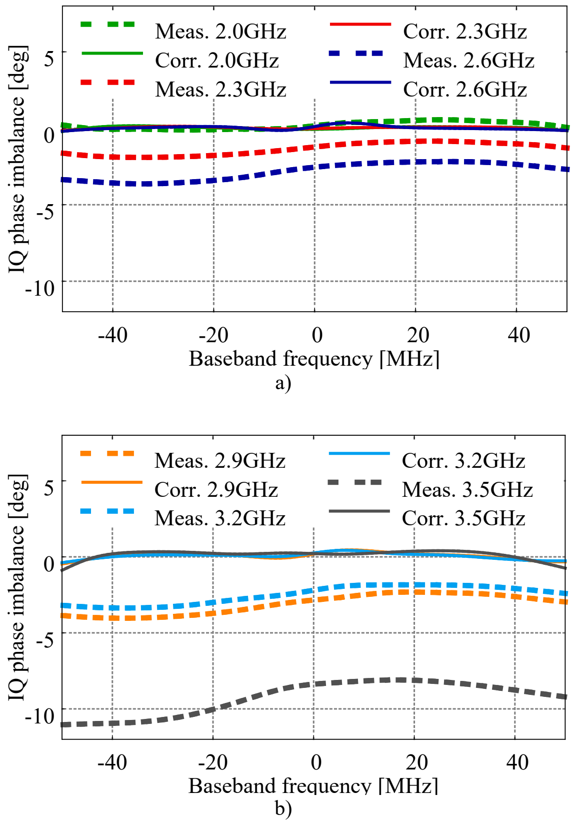

Fig. 10. RX phase IQI measured at a) 2.0 GHz, 2.3 GHz, 2.6 GHz; b) 2.9 GHz, 3.2 GHz and 3.5 GHz.

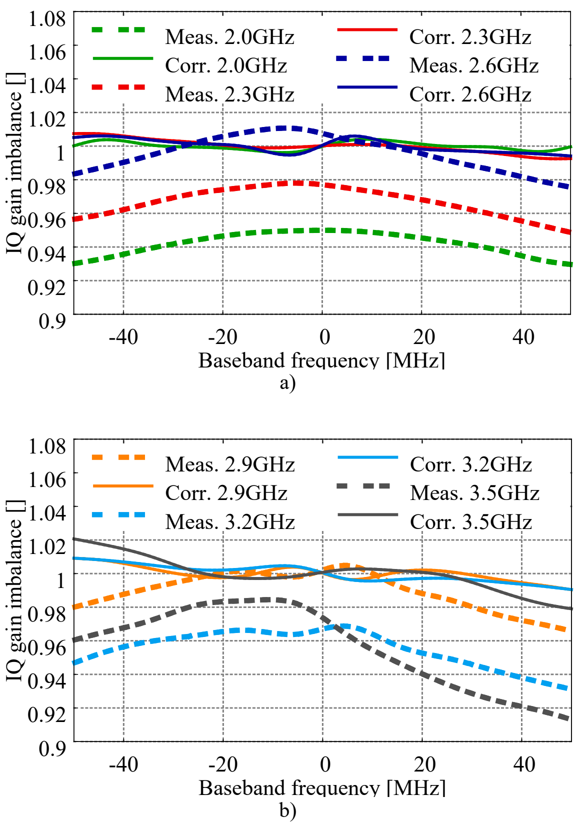

Fig. 11. RX gain IQI as a function of f_{BB} at a) 2.0 GHz, 2.3 GHz, 2.6 GHz; b) 2.9 GHz, 3.2 GHz, 3.5 GHz.

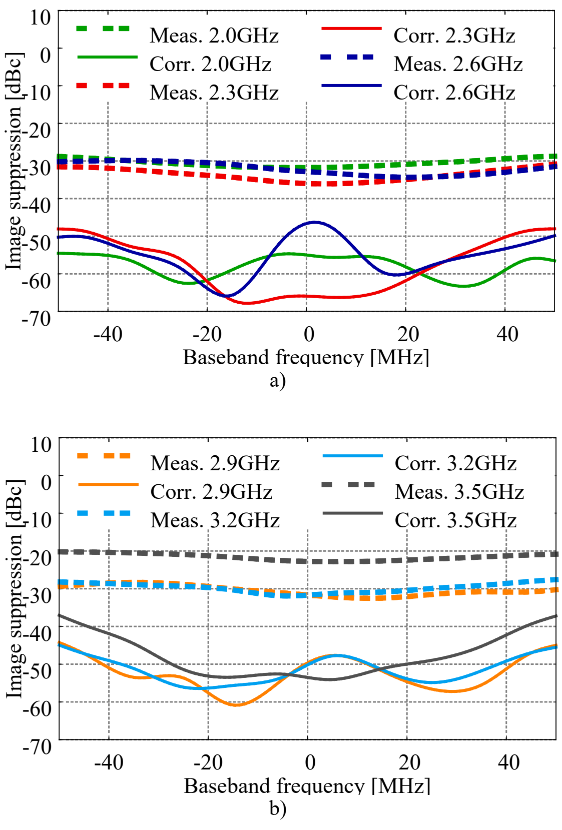

Fig. 12. The RX IQ image suppression at a) 2.0 GHz, 2.3 GHz, 2.6 GHz; b) 2.9 GHz, 3.2 GHz and 3.5 GHz.

The RX image suppression level is shown in Fig. 12. Single tone signals are produced by RF signal generator starting from RX_f_{LO} −50 MHz to RX_f_{LO} +50 MHz with the increment step of 5 MHz. The amplitude of test signals is equal to −30 dBm. The signals are then fed to the input of SDR receiver which LO is tuned to RX_f_{LO}. At each f_{BB}, the amplitudes of the main test tone, positioned at $RX\_f_{LO}+f_{BB}$, and the image component, positioned at $RX\_f_{LO}-f_{BB}$ are determined.

5. Discussion

A novel method for correction of the FS IQI is presented. The method relies on utilization of single tone test signals and spectral analysis for IQI extraction. Both receiver and transmitter IQ imbalances are calibrated for the baseband signal bandwidth of 100 MHz.

The IQI is reduced and the amplitude response is flattened. The advantage of the proposed method compared to the methods found in literature is that the hardware overhead is minimized. This is achieved by employing the transmitter as a test signal generator. Also, the receiver plays the role of a measuring device.

The RF signal loopback, implemented by on-board RF switches, represents the only additional hardware which supports the calibration process. The calibration is executed at the transceiver start-up and can be periodically repeated. Special factory or laboratory calibration is not required.

Reduction of FIR filter length enables savings of FPGA resources, which makes the method suitable for realization in FPGA. It is worth mentioning that beside the proposed FS IQ corrector, the other digital blocks are also required in transmitter paths, such as crest factor reduction (CFR) and post-CFR FIR filters. For implementation of these digital blocks, significant amount of FPGA resources is spent [27]. Moreover, the hardware is optimized to occupy minimum resources on FPGA for transceiver 2×2 MIMO operation.

When gain and phase imbalance functions are symmetrical a real-valued digital filter can be utilized for FS IQ mitigation. However, when these criteria are not fulfilled, a complex filter is required. As measured results proved, at central frequencies greater than 3 GHz, the TX and RX gain imbalance functions are asymmetrical. In order to reduce the asymmetry, compared to the symmetrical form given by (7), the adopted $\gamma(\omega)$ is designed to incorporate odd polynomial elements with exponents equal to 1 and 3 (8). The results showed that the receiver $\varphi(\omega)$ becomes asymmetrical at f_{LO} greater than 3 GHz. At same frequencies the TX $\varphi(\omega)$ doesn't possess this property. Compared to the symmetric form given in (9), the implemented $\varphi(\omega)$ (10), includes even polynomial parts whose exponents are equal to 2 and 4.

The complex filter is designed based on previously determined IQ imbalance models. It consists of four real valued FIR filters. Two FIR filters are positioned in I and Q paths. The others are located in cross paths (see Fig. 1). Digital differentiator and fractional delay FIR filters are used for realization of cross path filters. They cancel the asymmetric portion of IQI. Specifically, the gain of cross path filters compensates the odd part of $\gamma(\omega)$. The even part of $\varphi(\omega)$ function is neutralized by the phase difference which is introduced by the delay between cross path filter impulse responses.

The method performance is assessed at different f_{LO}, starting from 2 GHz to 3.5 GHz. The IRR of the uncalibrated transmitter ranges between 20 dBc and 35 dBc, depending on f_{LO}. Different configurations of compensation circuits are investigated. First, the performance is estimated of the circuit consisting only of two real valued FIR filters, positioned in I and Q signal paths. The measured results proved that when transceiver LO is tuned at higher LO frequencies the utilization of real valued FIR_II and FIR_QQ cannot remove the IQ images. For example, at f_{LO} = 3.5 GHz, after calibration is done, the resulting TX IRR is only 38 dBc. The utilization of complex filters gives better results. When the proposed method is applied, the corrected amplitude response becomes flatter than in the case of uncalibrated transmitter. Also, the corrected phase and gain IQI become closer to the ideal values over the entire pass band of 100 MHz. When TX IQI is corrected (given in Fig. 1) the IRR is improved by more than 25 dBc. The resulting IRR reaches 45–50 dBc.

The RX measured results confirm improvement in IQ image rejection. The measured IRR of uncalibrated receiver, operating at LO frequencies less than 3.5 GHz, is approximately equal to 30 dBc. At f_{LO} = 3.5 GHz, the IRR is only 20 dBc. After the proposed method is applied, the corrected phase IQI values get close to zero degrees. Also, the corrected $\gamma(\omega)$ gets near to the ideal case. By applying the RX IQ complex filter, the IRR becomes greater than 50 dBc. The improvement at f_{LO} = 3.5 GHz is more than 30 dBc.

The methods from literature are focused on either receiver or transmitter calibration. In our case the imbalances of both receiver and transmitter are corrected. The TX IQI mitigation techniques which are found in literature require implementation of additional hardware for IQI detection. The monitoring path is realized by external instruments or dedicated ADCs [28]. The measured results are produced using laboratory equipment that relies on high-performance signal generators. Moreover, the calibration procedures are realized in MATLAB. In [29] the TX mitigation method improves the IRR over 45 dBc. When a ten-tone waveform is applied, the method yields increase in IRR by 10–15 dBc [29]. In [13] 10 dBc IRR enhancement is achieved for a baseband signal bandwidth of 80 MHz. The algorithm gives more than 50 dBc IRR on both sidebands which indicates that the FS IQI is mitigated well. In [18] the experimental results give the receiver IRR improvement of 30 dBc compared to uncompensated case. The disadvantage of the method from [18] is that it does not utilize complex filters, and therefore, cannot neutralize asymmetric IQI. The RX IQI reduction procedure from [20] provides the IRR better than 65 dBc over 600 MHz bandwidth for a transceiver operating in 1 GHz to 6 GHz frequency range. The comparison of the proposed method with the results found in literature is given in Tab. 1.

		Ref. [13]	Ref. [18]	Ref. [20]	Ref. [29]	Proposed
Signal bandwidth [MHz]		150	200	600	400	**100**
Central frequency [GHz]		1	3	1–6	11	**2.0–3.5**
TX	**Sample rate [MS/s]**	10000	/	/	800	**245.76**
	Before comp. IRR [dBc]	40–45	/	/	20	**20–30**
	After comp. IRR [dBc]	50–55	/	/	45	**45–55**
RX	**Sample rate [MS/s]**	/	491.7	1250		**122.88**
	Before comp. IRR [dBc]	/	52.2	25–40		**20–30**
	After comp. IRR [dBc]	/	81.6	65		**40–60**

Tab. 1. Performance comparison of different methods.

6. Conclusion

In the paper the method for compensation of wideband transceiver IQ impairments is described. The method corrects the imbalances of both the receiver and transmitter. The measured results that are presented in the paper are obtained after the method has been implemented in a SDR-based RF transceiver. Particularly, the transceiver is used for transmission of the wideband modulation waveforms; it operates at a central frequency of 3.5 GHz where the transmitted signal bandwidth is 100 MHz. The advantage of the method is that it does not require special hardware for calibration operations. The RF loopback is added to support the calibration process. In calibration setup the transmitter is utilized as a test signal generator, while the receiver is a measuring device. The method performance is assessed by IRR measurements. The IRR is measured in cases when the transceiver is tuned to different LO frequencies, starting from 2.0 GHz to the target frequency of 3.5 GHz. The results prove efficient IQ imbalance suppression increasing the quality of wideband signals. The design methodology is generic and the proposed solution is suitable for implementation in other field-programmable RF base stations. For the future work the development of a method that mitigates the IQ impairments which appear in massive MIMO transceivers is envisaged.

Acknowledgments

This research was funded by The Ministry of Education, Science and Technological Development of the Republic of Serbia.

References

[1] CAVERS, J. K., LIAO, M. W. Adaptive compensation for imbalance and offset losses in direct conversion transceivers. *IEEE Transactions on Vehicular Technology*, 1993, vol. 42, no. 4, p. 581–588. DOI: 10.1109/25.260752

[2] RAZAVI, B. Design considerations for direct-conversion receivers. *IEEE Transactions on Circuits and Systems II: Analog and Digital Signal Processing*, 1997, vol. 44, no. 6, p. 428–435. DOI: 10.1109/82.592569

[3] VALKAMA, M. *Advanced I/Q Signal Processing for Wideband Receivers: Models and Algorithms*. Ph.D. dissertation. Tampere (Finland): Tampere University of Technology, 2001. ISBN: 9521507152

[4] 3GPP. *Technical Specification Group Radio Access Network; NR; Base Station (BS) Radio Transmission and Reception.* 2019, Valbonne, France, Tech. Rep.

[5] KISS, P., PRODANOV, V. One-tap wideband I/Q compensation for zero-IF filters. *IEEE Transactions on Circuits and Systems I: Regular Papers*, 2004, vol. 51, no. 6, p. 1062–1074. DOI: 10.1109/TCSI.2004.829233

[6] LIM, A. G. K. C., SREERAM, V., WANG, G. Q. Digital compensation in IQ modulators using adaptive FIR filters. *IEEE*

Transactions on Vehicular Technology, 2004, vol. 53, no. 6, p. 1809–1817. DOI: 10.1109/TVT.2004.836934

[7] TUTHILL, J. CANTONI, A. Efficient compensation for frequency-dependent errors in analog reconstruction filters used in IQ modulators. *IEEE Transactions on Communications*, 2005, vol. 53, no. 3, p. 489–496. DOI: 10.1109/TCOMM.2005.843455

[8] DING, L., MA, Z., MORGAN, D. R., et al. Compensation of frequency-dependent gain/phase imbalance in predistortion linearization systems. *IEEE Transactions on Circuits and Systems I: Regular Papers*, 2008, vol. 55, no. 1, p. 390–397. DOI: 10.1109/TCSI.2007.910545

[9] ANTTILA, L., VALKAMA, M., RENFORS, M. Frequency-selective IQ mismatch calibration of wideband direct-conversion transmitters. *IEEE Transactions on Circuits and Systems II: Express Briefs*, 2008, vol. 55, no. 4, p. 359–363. DOI: 10.1109/TCSII.2008.919500

[10] CAVERS, J. K. The effect of quadrature modulator and demodulator errors on adaptive digital predistorters for amplifier linearization. *IEEE Transactions on Vehicular Technology*, 1997, vol. 46, no. 2, p. 456–466. DOI: 10.1109/25.580784

[11] ANTTILA, L., HANDEL, P., VALKAMA, M. Joint mitigation of power amplifier and I/Q modulator impairments in broadband direct-conversion transmitters. *IEEE Transactions on Microwave Theory and Techniques*, 2010, vol. 58, no. 4, p. 730–739. DOI: 10.1109/TMTT.2010.2041579

[12] CAO, H., SOLTANI TEHRANI, A., FAGER, C., et al. I/Q imbalance compensation using a nonlinear modeling approach. *IEEE Transactions on Microwave Theory and Techniques,* 2009, vol. 57, no. 3, p. 513–518. DOI: 10.1109/TMTT.2008.2012305

[13] LI, W., ZHANG, Y., HUANG, L. K., et al. Self-IQ-demodulation based compensation scheme of frequency-dependent IQ imbalance for wideband direct-conversion transmitters. *IEEE Transactions on Broadcasting*, 2015, vol. 61, no. 4, p. 666–673. DOI: 10.1109/TBC.2015.2465138

[14] MKADEM, F., FARRES, M. C., BOUMAIZA, S., et al. Complexity reduced Volterra series model for power amplifier digital predistortion. *Analog Integrated Circuits and Signal Processing,* 2014, vol. 79, p. 331–343. DOI: 10.1007/s10470-014-0266-4

[15] VALKAMA, M., RENFORS, M., KOIVUNEN, V. Blind source separation based I/Q imbalance compensation. In *Proceedings of the IEEE 2000 Adaptive Systems for Signal Processing, Communications, and Control Symposium*. Lake Louise (Canada), 2000, p. 310–314. DOI: 10.1109/ASSPCC.2000.882491

[16] CETIN, E., KALE, I., MORLING, R. Adaptive compensation of analog front-end I/Q mismatches in digital receivers. In *Proceedings of 2001 IEEE International Symposium on Circuits and Systems (ISCAS 2001).* Sydney (Australia), 2001, vol. 4, p. 370–373. DOI: 10.1109/ISCAS.2001.922250

[17] ZEKKARI, C., DJENDI, M., GUESSOUM, A. Efficient adaptive filtering algorithm for IQ imbalance compensation TX/RX systems. *IET Signal Processing,* 2018, vol. 12, no. 5, p. 566–573. DOI: 10.1049/iet-spr.2017.0448

[18] PENG, X., WANG, Z., MO, J., et al. A blind calibration model for I/Q imbalances of wideband zero-IF receivers. *Electronics*, 2020, vol. 9, no. 11, p. 1–16. DOI: 10.3390/electronics9111868

[19] LI, Y., CHEANG, C. F., MAK, P. I., et al. Joint-digital-predistortion for wireless transmitter's I/Q imbalance and PA nonlinearities using an asymmetrical complexity-reduced Volterra series model. *Analog Integrated Circuits and Signal Processing*, 2016, vol. 87, no. 1, p. 35–47. DOI: 10.1007/s10470-016-0724-2

[20] ROSOLOWSKI, D. W., KORPAS, P. IQ-imbalance and DC-offset compensation in ultra wideband zero-IF receiver. In *Proceedings of the 23rd International Microwave and Radar Conference (MIKON)*. Warsaw (Poland), 2020, p. 209–213. DOI: 10.23919/MIKON48703.2020.9253894

[21] MENG, J., WANG, H., YE, P., et al. I/Q linear phase imbalance estimation technique of the wideband zero-IF receiver. *Electronics*. 2020, vol. 9, no. 11, p. 1–14. DOI: 10.3390/electronics9111787

[22] JOVANOVIĆ, B., MILENKOVIĆ, S. Transmitter IQ imbalance mitigation and PA linearization in software defined radios. *Radioengineering*, 2022, vol. 31, no. 1, p. 144–154. DOI: 10.13164/re.2022.0144

[23] INGLE, V. K., PROAKIS, J. G. *Digital Signal Processing Using MATLAB: A Problem Solving Companion*. 4th ed. Boston (USA): Cengage Learning, 2015. ISBN: 978-1305635128

[24] FLETCHER, R. *Practical Methods of Optimization.* 2nd ed. New York (USA): John Wiley & Sons, 1987. ISBN: 978-0-471-91547-8

[25] LIMEMICROSYSTEMS, UK. *LimeSDR qPCIe* (datasheet). [Online] Cited 2023-06-28. Available at: https://wiki.myriadrf.org/LimeSDR-QPCIe

[26] KIELA, K., JURGO, M., MACAITIS, V., et al. 5G standalone and 4G multi-carrier network-in-a-box using a software defined radio framework. *Sensors*, 2021, no. 21, p. 1–18. DOI: 10.3390/s21165653

[27] JOVANOVIĆ, B., MILENKOVIĆ, S. PA linearization by digital predistortion and peak to average power ratio reduction in software defined radios. *Journal of Circuits, Systems and Computers*, 2020, vol. 29, no. 9, p. 1–19. DOI: 10.1142/S0218126620501479

[28] FAN, L., LI, Y. ZHAO, M. Joint IQ imbalance and PA nonlinearity pre-distortion for highly integrated millimetre-wave transmitters. In *Proceedings of 2014 IEEE Globecom Workshops (GC Wkshps)*. Austin (USA), 2014, p. 399–404. DOI: 10.1109/GLOCOMW.2014.7063464

[29] KIM, M., MARUICHI, Y., TAKADA, J. I. Parametric method of frequency dependent I/Q imbalance compensation for wideband quadrature modulator. *IEEE Transactions on Microwave Theory and Techniques*, 2013, vol. 61, no. 1, p. 270–280. DOI: 10.1109/TMTT.2012.2228215

About the Authors ...

Borisav JOVANOVIĆ was born in 1979 in Niš, Republic of Serbia. He received his Ph.D. degree from the Dept. of Electronics, Faculty of Electrical Engineering, University of Niš, Serbia, in 2016, which is entitled with *"Advanced Methods of Designing Digital Integrated Circuits in Nanometer Technologies with Special Emphasis on Speed, Static and Dynamic Consumption"*. His current research is focused on digital techniques for predistortion and correction of static and dynamic IQ imbalance of 4G and 5G RF transmitters.

Srđan MILENKOVIĆ was born in 1962 in Leskovac, Republic of Serbia. He received his Ph.D. degree from the Dept. of Electronics, Faculty of Electrical Engineering, University of Niš in 1996 and his Ph.D. thesis deals with artificial neural networks. His research is focused on the design of software radio defined telecommunication systems.